THE JOURNAL OF PHYSICAL CHEMISTRY C

Article

pubs.acs.org/JPCC

Understanding the Phase Diagram of Self-Assembled Monolayers of Alkanethiolates on Gold

Joakim Löfgren,*[,†] Henrik Grönbeck,[†] Kasper Moth-Poulsen,[‡] and Paul Erhart[†]

[†]Department of Physics and [‡]Department of Chemistry and Chemical Engineering, Chalmers University of Technology, Gothenburg, Sweden

ABSTRACT: Alkanethiolate monolayers on gold are important both for applications in nanoscience as well as fundamental studies of adsorption and self-assembly at metal surfaces. While considerable experimental effort has been put into understanding the phase diagram of these systems, theoretical work based on density functional theory (DFT) has long been hampered by the inability of conventional exchange-correlation functionals to describe dispersive interactions. In this work, we combine dispersion-corrected DFT calculations using the new vdW-DF-CX functional with the ab initio thermodynamics method to study the stability of dense standing-up and low-coverage lying-down phases on Au(111). We demonstrate that the lying-down phase has a thermodynamic region of stability starting from thiolates with alkyl chains consisting of $n \approx 3$ methylene units. This phase emerges as a consequence of a competition between dispersive chain−chain and chain−substrate interactions, where the strength of the latter varies more strongly with n. A phase diagram is derived under ultrahigh-vacuum conditions, detailing the phase transition temperatures of the system as a function of the chain length. The present work illustrates that accurate ab initio modeling of dispersive interactions is both feasible and essential for describing self-assembled monolayers.

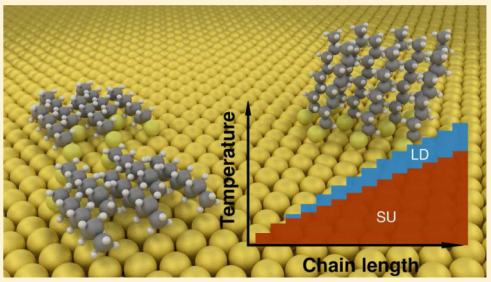

INTRODUCTION

Self-assembled monolayers (SAMs) play a central role in modern surface chemistry and nanoscience with a wide range of applications in e.g. medicine, sensing, molecular electronics, and catalysis.[1−5] In this context, alkanethiolates on the Au(111) surface are representative of a large class of SAMs formed by adsorbates with a headgroup that has a strong interaction with the substrate, a hydrocarbon backbone, and an end-group possibly providing functionalization. SAMs on low-index metal facets such as Au(111) can also be considered as prototypes for ligand-functionalized nanoparticles,[6−8] which are an important subset of SAM systems.

A key challenge for experimental and theoretical studies alike is to map out the phase diagram of SAMs as a function of the chemical environment and the length of the alkyl chain. From a theoretical perspective, the main tool in analyzing the stability of different surface structures is provided by density functional theory (DFT), for which a longstanding issue is the treatment of dispersive, or van der Waals (vdW), interactions. This has put severe limitations on predictions made for alkyl chains extending beyond one or two methylene units. Here we demonstrate with the aid of recent advances in dispersion-corrected DFT a quantitative ab initio description of the phase diagram of alkanethiolate SAMs on Au(111). In addition to providing new insight into the system, this establishes a stepping stone for future work aimed at understanding SAMs in general.

Stable alkanethiolate SAMs are readily prepared from solution under ambient conditions or from physical vapor deposition in ultrahigh vacuum (UHV).[1] The preparation can start either from thiols, RSH, or dialkyl disulfides, $(RS)_2$, where $R = R_n \equiv (CH_2)_nCH_3$. In either case, the molecules will adsorb dissociatively as thiolates. It was initially uncovered that this could lead to at least two types of high coverage SAM structures. In the simplest case, the thiolates are arranged in a $(\sqrt{3} \times \sqrt{3})R30°$ structure.[9,10] The other possibility involves more complicated geometries described by a $(3 \times 2\sqrt{3})$rect unit cell or, equivalently, a $c(4\sqrt{3} \times 2\sqrt{3})R30°$ cell.[11,12] It is common to reference this structure to the $(\sqrt{3} \times \sqrt{3})R30°$ mesh, rather than the primitive mesh as typically done with Wood's notation. Accordingly, it is denoted "$c(4 \times 2)$", here surrounded by quotation marks as a reminder of the nonprimitive reference mesh. In both the $(\sqrt{3} \times \sqrt{3})R30°$ and the "$c(4 \times 2)$" structure, the molecules adopt standing-up (SU) configurations with the molecular axes tilted by about 30° off the surface normal.[13] It should be noted that these two, however, are not the only possible saturation coverage structures. For short chain alkanethiolates with no more than one CH_2 unit, a 3×4 structure has been reported as stable up to room temperatures.[14−16]

In order to reconcile conflicting data regarding the preferred binding site of the thiolates, it was later proposed that the surface may reconstruct upon adsorption.[17−23] For the "$c(4 \times 2)$" structure, adsorption geometries involving RS−Au−SR complexes have been shown to match experimental data[22,24−26]

Received: March 31, 2016
Revised: May 11, 2016
Published: May 12, 2016

DOI: 10.1021/acs.jpcc.6b03283
J. Phys. Chem. C 2016, 120, 12059−12067

in addition to being energetically favorable compared to other proposals according to DFT calculations.[5,27]

The phase diagram is further complicated by the existence of an ordered lying-down (LD), or striped, phase present at low-coverage for thiolates with medium to long alkyl chains. The LD phase structures are characterized by the adsorbate molecular axes being nearly parallel to the surface and frequently studied chain lengths include n = 5, 7, 9, and 11.[28−31] While the phase behavior varies with the number of CH_2 units, many of the observed LD structures can be described by unit cells of the form $(p \times \sqrt{3})$rect where p is such that the resulting periodicity is roughly twice the length of the fully extended thiolate.[28,32]

To probe the phase diagram with DFT calculations, one must be able to account for (1) the metallic bonding in the gold substrate, (2) the covalent bonding in the alkyl chain as well as between the headgroup and the surface, and (3) the dispersive chain−chain and chain−substrate interactions. This poses a formidable challenge since in conventional exchange-correlation (XC) functionals of e.g. GGA-type the dispersive interactions are omitted by construction. However, during the past two decades, several methods[33−37] with various level of sophistication have been proposed for dispersion-corrected DFT calculations. A rigorous approach is provided by the van der Waals density functional (vdW-DF) framework[38−40] where a suitable GGA-type exchange functional is augmented with a nonlocal correlation term.[41] One of the advantages with this approach is that the first-principles nature, and therefore also the predictive power, of the calculation is preserved.

Previously, the thermodynamics of short-chain SU phase structures has been investigated[42,43] using the ab initio thermodynamics method.[44−46] This approach enables the determination of the stability of adsorbate structures with different coverage and under variable thermodynamic conditions. What has been missing, however, is the extension of such an analysis to long-chain alkanethiolates, where vdW interactions must be properly accounted for in order to describe the LD and SU phases. While previous dispersion-corrected DFT studies have been devoted to understanding the geometry and interaction in SU structures, the LD phase has rarely been addressed[47] and not from a thermodynamic perspective. In the present work, our objective is to provide a phase diagram that includes both LD and SU phases.

To describe the different interactions in the system on an equal footing, we employ the recently developed vdW-DF-CX (CX) functional.[48] This allows for the calculation of the adsorption energy scaling with chain length, n, in both the SU and LD phases. Such calculations have previously been carried out for the SU phase using empirical corrections[47,49] as well as earlier incarnations of the vdW-DF functional,[50] but no firm connection to experimental results has been made. After establishing the n-dependence of the adsorption energy in the LD and SU phases, we show that a decisive comparison to experiment can be made. Using the adsorption data as input to an ab initio thermodynamics model yields a quantitative picture of the origin of dispersion-driven phase transitions in alkanethiolate SAMs as a function of the chemical environment. In particular, an (n, T) phase diagram is constructed and we show qualitatively the impact of the conformational entropy on the final shape of the phase boundaries.

METHODOLOGY

Thermodynamical Model. In this section we review the thermodynamical model employed to study the energetics and phase stability of alkanethiolate SAMs on Au(111). We consider an interface region of Au(111) surface in contact with a gas-phase reservoir of $(RS)_2$ molecules, which can absorb dissociatively on the surface. In the simple case of two adsorbate structures with identical coverage, the stable structure at arbitrary (T, p) is determined by the adsorption energy

$$\Delta E_{ads} = E_{surf:RS} - E_{surf} - \frac{1}{2}N_{RS}E_{(RS)_2} - \Delta N_{Au}E_{Au}^{bulk} \quad (1)$$

where $\Delta E_{ads} < 0$ is the condition for exothermic adsorption with respect to the clean, unreconstructed surface. On the right-hand side of eq 1, $E_{surf:RS}$ is the energy of the surface plus adsorbate system, E_{surf} is the energy of the clean surface, $E_{(RS)_2}$ is the energy of a $(RS)_2$ molecule in vacuum, and N_{RS} is the number of adsorbed thiolate fragments. The last term accounts for the possibility of surface reconstructions upon adsorption and is given by the bulk energy per gold atom E_{Au}^{bulk} times the change in the number of gold atoms ΔN_{Au}. We express this change as $\Delta N_{Au} = N_a - N_v$, where N_a is the number of adatoms and N_v is the number of vacancies. It is convenient to also define the average adsorption energy per thiolate fragment

$$\mathcal{E}_{ads} = \frac{\Delta E_{ads}}{N_{RS}} \quad (2)$$

and for the remainder of this text we shall take the term adsorption energy to refer to this expression instead of eq 1.

When examining the relative stability of the SU and LD phases, it becomes necessary to compare structures with different coverage. The quantity that must then be minimized is not the adsorption energy but rather the surface free energy γ_{ads}. If the adsorbate structures share the same underlying crystal facet, in the present case {111}, it suffices to consider $\Delta\gamma_{ads}$, the surface free energy relative to that of the clean surface. The change in Gibbs free energy corresponding to the formation of an adsorbate phase of area A is then given by $\Delta G = A\Delta\gamma_{ads}$. The surface free energy can be calculated as

$$\Delta\gamma_{ads}(T, p) \approx \frac{N_{RS}}{A}(\mathcal{E}_{ads} - N_{RS}\mu_{RS}(T, p)) \quad (3)$$

which is a linear function of the chemical potential of the gas-phase μ_{RS} that contains all the temperature and pressure dependence. The slope of the line is directly proportional to the coverage $\Theta = N_{RS}A_{prim}/A$, where A_{prim} is the area of the primitive surface cell. If, on the other hand, the underlying crystal facets are not identical, differences in the energy of the clean surfaces must be accounted for and the total surface free energy

$$\gamma_{ads}(T, p) = \gamma_{clean}^{hkl}(T, p) + \Delta\gamma_{ads}^{hkl}(T, p) \quad (4)$$

is minimized instead. For a general set of adsorbate structures, the thermodynamic stability can be compactly represented by taking the convex hull of the corresponding set of $(\gamma_{ads}, \mu_{RS}^{gas})$ lines.

In eq 3 several contributions, chiefly vibrational in nature, to the free energy are neglected as indicated by the approximate equality. This is motivated by the fact that the full surface free energy contains differences between similar terms, for which it is reasonable to assume a partial cancellation. For instance, the

DOI: 10.1021/acs.jpcc.6b03283
J. Phys. Chem. C 2016, 120, 12059−12067

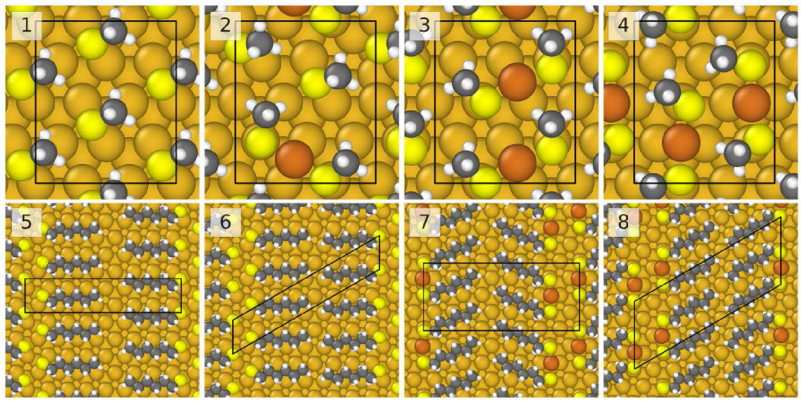

Figure 1. Eight different adsorption geometries for the standing-up and lying-down phases on Au(111). The standing-up structures **1**−**4** have unit cells that are independent of chain length, illustrated here for adsorption of methylthiolate. **5**−**8** feature hexanethiolate in the lying-down phase, for which the unit cells are specific to the chain length. The atoms are colored according to Au (gold), C (gray), H (white), S (yellow), and Au adatom (red).

difference in vibrational entropy between a molecule on the surface and a molecule in the reservoir is often small.

The remaining free energy contributions from the gas-phase are contained in the relative chemical potential μ_{RS}, which assuming ideal-gas behavior, takes the form

$$\mu_{RS}(T, p) = \frac{1}{2}\left(\mu^{gas}_{(RS)_2}(T, p^\circ) + k_B T \ln\left(\frac{p}{p^\circ}\right)\right) \quad (5)$$

Here, $\mu^{gas}_{(RS)_2}(T,p^\circ)$ is composed of the translational and rotational contributions at the reference pressure p° = 1 atm.

So far we have not taken into account the configurational entropy, which enters in the surface free energy as a difference between adsorbates and molecules in the reservoir. While this contribution is small for short alkyl chains, the same cannot be expected when the chain length increases, since molecules in a monolayer structure are much more limited to adopt different conformations. For gas-phase alkanes and related compounds such as thiols, one can use a simple rotational isomeric state model[51,52] to estimate the conformational free energy. In this model the number of conformations achievable by applying one or more gauche(±) defects along an all-trans alkyl chain are counted. The partition function is given by

$$\mathcal{Z} = \frac{1}{2}\left({x_1}^{n-1} + {x_2}^{n-1} + \frac{1-w}{x_1 - x_2}({x_1}^{n-1} - {x_2}^{n-1})\right) \quad (6)$$

In this expression, $w = \exp(-\Delta E_g/k_B T)$ where ΔE_g denotes the formation energy of a gauche defect and $x_{1,2} = 1 + w \pm (1 + 6w + w^2)^{1/2}$.

Computational Setup. The total energies were evaluated by means of DFT calculations using the Vienna ab initio simulation package[53] (version 5.3.3), which uses plane wave basis sets[54] and the projector augmented wave method.[55,56] To give an accurate description of the different interactions in the system, the CX functional[48] was employed, which was recently implemented in VASP.[57] For comparison, a subset of the calculations were also carried out with the PBE functional.[58]

The clean and the adsorbate-covered surfaces were represented using slab models consisting of five atomic layers of gold and one adsorbate-covered side. A vacuum region of 16 Å was introduced in the direction of the surface normal. Similarly, the energies of the free dialkyl disulfides were calculated in a cubic cell with a side length of 16 Å. The calculations were performed with a plane wave cutoff energy of 400 eV and the Gaussian electronic-smearing scheme of width σ = 0.2 eV. The atomic positions were allowed to relax until the forces were less than 20 meV/Å. Adsorption of alkanethiolates was investigated for both SU and LD phases. The SU phase structures were realized in $(3\times 2\sqrt{3})$rect unit cells to ensure as much error cancellation as possible and a 4 × 4 × 1 Monkhorst−Pack grid was used for Brillouin zone integrations. In the LD phase, the computational expense grows rapidly with increasing chain length. For this reason, minimal unit cells were used for all the LD phase calculations. In the case of hexanethiolate adsorption, this included unit cells of $(8 \times \sqrt{3})$rect, $(8 \times 2\sqrt{3})$rect, $(5\sqrt{3} \times \sqrt{3})R30°$, and $(5\sqrt{3} \times 2\sqrt{3})R30°$, for which the Brillouin zone integration was carried out on 2 × 8 × 1, 2 × 4 × 1, 2 × 8 × 1, and 2 × 4 × 1 k-point grids, respectively. Configurations were analyzed and visualized using OVITO.[59]

RESULTS AND DISCUSSION

Bare Substrate. Lattice constants of a_0^{CX} = 4.09 Å and a_0^{PBE} = 4.16 Å were calculated by relaxing the Au bulk fcc structure. The experimental value is a_0^{exp} = 4.078 Å,[60] and thus CX significantly mitigates the overestimation of the lattice constant characteristic of PBE calculations of Au. It turns out that CX also gives a better description of the energetics of the gold surface as illustrated by the surface energy of the clean gold (111) facet, denoted γ^{111}_{clean}. A value of $\gamma^{111}_{clean}(CX)$ = 1.19 J/m^2 was calculated with CX while the corresponding PBE value is $\gamma^{111}_{clean}(PBE)$ = 0.71 J/m^2. A comparison to the experimental value $\gamma^{111}_{clean}(exp)$ = 1.50 J/m^2 given in ref 61 demonstrates that CX represents a significant improvement compared to PBE. These results suggest that caution has to be taken when comparing reconstructed and unreconstructed surfaces at the PBE level. Some of the earlier versions of the vdW-DF functional also give unreliable descriptions of the gold substrate, for instance with the original vdW-DF1[38] a_0^{DF1} = 4.24 Å and $\gamma^{111}_{clean}(DF1)$ = 0.69 J/m^2.

Adsorption Geometries. A total of eight different adsorption geometries were investigated for the LD and SU phases (Figure 1). The saturation coverage geometries **1**−**4** have been suggested in previous studies;[26,62,63] they are shown here for the case of methylthiolate (MT) adsorption to provide an unobstructed view of the binding to the substrate. As the chain length increases, the unit cells remain unchanged and the

DOI: 10.1021/acs.jpcc.6b03283
J. Phys. Chem. C 2016, 120, 12059−12067

Table 1. Summary of the Basic Structural Information and Energetics of the Investigated Adsorption Geometries 1−8[a]

				$\mathcal{E}_{ads}$ (eV)		$\mathcal{E}_{ads} - \mathcal{E}_{ads}^{ref}$ (eV)		$\mathcal{E}_{ads}/A$ (meV/Å^2)
n	structure	minimal unit cell	Θ	CX	PBE	CX	PBE	CX
0	**1**	$(\sqrt{3} \times \sqrt{3})R30°$	1/3	−0.78	−0.30	+0.13	+0.27	−35.8
	2	$(3 \times 2\sqrt{3})$rect[b]	1/3	−0.79	−0.39	+0.12	+0.18	−36.1
	3	$(3 \times \sqrt{3})$rect	1/3	−0.87	−0.55	+0.04	+0.02	−40.1
	4	$(3 \times 2\sqrt{3})$rect	1/3	−0.91	−0.57	0	0	−42.0
5	**5**	$(8 \times \sqrt{3})$rect	1/8	−1.44		+0.05		−24.8
	6	$(5\sqrt{3} \times \sqrt{3})R30°$	2/15	−1.45		+0.04		−26.7
	7	$(8 \times 2\sqrt{3})$rect	1/8	−1.48		+0.01		−25.5
	8	$(5\sqrt{3} \times 2\sqrt{3})R30°$	2/15	−1.49		0		−27.4

[a]The first four columns contains the chain length, the index in Figure 1, the minimal unit cell, and the coverage. The next two columns list the adsorption energy per molecule, both as an absolute value and relative to the most stable geometry. The final column is the surface averaged adsorption energy. [b]Equivalent to "$c(4 \times 2)$".

thiolates adopt their characteristic, slightly tilted, SU configurations. **1** is a $(\sqrt{3} \times \sqrt{3})R30°$ structure realized in a larger $(3 \times 2\sqrt{3})$rect unit cell to facilitate comparison with the "$c(4 \times 2)$" structure. There are four MT molecules adsorbed at bridge-fcc positions. The remaining SU geometries **2**−**4** are all candidates for the "$c(4 \times 2)$" structure. **2** features one RS−Au−SR complex for which the bonding of the sulfur atoms to the surface is mediated by an Au adatom while two MT molecules are adsorbed directly at the surface around a vacancy. In **3** and **4** there are instead two RS−Au−SR complexes per unit cell. **3** has the two complexes adsorbed in equivalent positions, in contrast to **4** where two nonequivalent positions are occupied. As previously mentioned, in the specific case of very short thiolates such as MT or ethylthiolate, there is evidence suggesting that a (3×4) structure with a geometry based on RS−Au−SR complexes is the true saturation coverage phase. For the intermediate chain lengths, with which we are primarily concerned with in this work, this phase is, however, superseded in favor of "$c(4 \times 2)$" structures.[64] Hence, we consider only the latter, which is relevant for the study of phase transitions between the LD and SU phases.

The geometries **5**−**8** show LD structures for hexanethiolate (HT). This particular chain length was chosen because it features pronounced dispersion effects and is a feasible target for DFT calculations in terms of system size. **5** has two HT molecules in a $(8 \times \sqrt{3})$rect unit cell and is a member of the $(p \times \sqrt{3})$rect family of structures. The thiolates are arranged in head-to-head configurations with the sulfur atoms forming rows along $\langle 12^{-}1 \rangle$. In addition to **5**, STM imaging has suggested the similar structure **6**, which has slightly higher coverage and can be described by a $(5\sqrt{3} \times \sqrt{3})R30°$ unit cell. **5** and **6** can be extended to the case of Au-adatom-mediated bonding as seen in **7** and **8**. Here, the RS−Au−SR complexes are found in head-to-head configurations and the unit cells are $(8 \times 2\sqrt{3})$rect and $(5\sqrt{3} \times 2\sqrt{3})R30°$, respectively.

Adsorption Energies. The adsorption energies of the geometries **1**−**8** are reported in Table 1 along with a summary of the minimal unit cells and coverage. Recalling the sign convention that $\mathcal{E}_{ads} < 0$ implies exothermicity, we see that among the SU phase structures **1**−**4** both CX and PBE predict that **4** is the most stable.[a] Although dispersion effects are not expected to be significant for adsorption of MT, the more accurate description of the gold substrate energetics obtained with CX alleviates some of the concern that PBE might yield a spurious ground state structure.

Clearly, there is a quantitative difference between CX and PBE in terms of the calculated adsorption energies, with CX consistently yielding larger values by a factor 2−3. Whether this difference puts the adsorption energies closer to experimental values is difficult to gauge. Temperature-programmed desorption (TPD) measurements[65] suggest that MT desorbs as dimethyl disulfide with a desorption energy of about 0.65 eV. This would indicate that CX overestimates the adsorption energy by either 0.1 or 0.26 eV comparing to **1** and **4**, respectively. The corresponding numbers for PBE are instead underestimations by 0.42 and 0.17 eV. As formation of a disulfide from the adsorbed thiolates requires several reaction steps, it is difficult from the TPD comparison alone to conclude which XC functional that most accurately describes the gold−sulfur bond.

In terms of the LD phase structures **5**−**8**, an adatom-based geometry **7**(**8**) is more stable than its unreconstructed equivalent **5**(**6**), which can be concluded based only on their $\mathcal{E}_{ads}$ values (Table 1). Note, however, that to compare the stability of **5** and **6** would strictly require us to look at the surface free energy since the coverage differs between the two. Furthermore, the overall differences in the adsorption energies are small, indicating that the energy landscape is relatively flat.

The presence of Au adatoms in the LD phase has previously been considered primarily on the basis of STM imaging.[22,66,67] Here, in addition to a lower adsorption energy (Table 1), another argument in favor of adatom-based adsorption geometries in the LD phase can be found by considering the preferred adsorption sites (Figure 1) where the two sulfur atoms in one unit cell are shifted asymmetrically off the bridge positions. In contrast, there is experimental data suggesting on-top adsorption of HT,[31] which would by our CX calculations, leads to an increase in adsorption energy by 0.08 eV. This discrepancy could be resolved with the adatom-based structures **7** and **8**, similarly to how adsorption geometries with RS−Au−SR complexes are proposed to solve the corresponding puzzle of the geometry of the "$c(4\times 2)$" structure.[68]

Chain Length Effects. To gain a quantitative understanding of the importance of dispersion interactions for alkanethiolate SAMs, we studied the chain length dependence of the adsorption energy. The $(\sqrt{3} \times \sqrt{3})R30°$ structure **1** and the most stable "$c(4 \times 2)$" structure **4** were selected to represent the SU phase (Figure 1), and their chains were extended up to a total of $n = 7$ methylene units (octanethiolates). For the LD phase, $(p \times 2\sqrt{3})$rect unit

DOI: 10.1021/acs.jpcc.6b03283
J. Phys. Chem. C 2016, 120, 12059−12067

cells were created to accommodate thiolates with adsorption geometries identical to that in **7** for n in the range 3−7.

The scaling of the respective adsorption energies with chain length (Figure 2) plainly illustrates the failure of PBE to describe dispersive interactions since no increase in stability is found going beyond methylthiolate. In contrast, CX yields adsorption energies that decrease approximately linearly with n for both the SU and the LD structures. By a careful comparison, it is possible to show that the CX result is in quantitative agreement with experimental data. The reference is provided by TPD measurements of desorption energies of alkanethiols RSH from a physisorbed state, implying that the binding comes purely from the chain−substrate (ch−sub) interaction which is estimated to be $\Delta\mathcal{E}^{\mathrm{phys}}_{\mathrm{ch-sub}} = -0.06$ eV/CH$_2$.[65] Turning to our CX calculations, the slope of the linear decrease of the adsorption energy (Figure 2), denoted $\Delta\mathcal{E}_{\mathrm{vdW}}$, represents the average change in adsorption energy per CH$_2$ unit. For the SU structures only chain−chain (ch−ch) interactions are present, and thus for **4** we have $\Delta\mathcal{E}^{\mathrm{SU}}_{\mathrm{vdW}} = \Delta\mathcal{E}^{\mathrm{SU}}_{\mathrm{ch-sub}} = -0.10$ eV/CH$_2$. In the LD phase, both ch−ch and ch−sub interactions contribute, yielding $\Delta\mathcal{E}^{\mathrm{LD}}_{\mathrm{vdW}} = \Delta\mathcal{E}^{\mathrm{LD}}_{\mathrm{ch-ch}} + \Delta\mathcal{E}^{\mathrm{LD}}_{\mathrm{ch-sub}} = -0.12$ eV/CH$_2$. Using the fact that a thiolate in a LD configuration only has half as many neighbors as it would have in a SU configuration, we can estimate $\Delta\mathcal{E}^{\mathrm{LD}}_{\mathrm{ch-sub}} = \Delta\mathcal{E}^{\mathrm{LD}}_{\mathrm{vdW}} - \Delta\mathcal{E}^{\mathrm{SU}}_{\mathrm{vdW}}/2 = -0.07$ eV/CH$_2$. Clearly, this value is in excellent agreement with the experimental $\Delta\mathcal{E}^{\mathrm{phys}}_{\mathrm{ch-sub}} = -0.06$ eV/CH$_2$, which measures the same interaction.

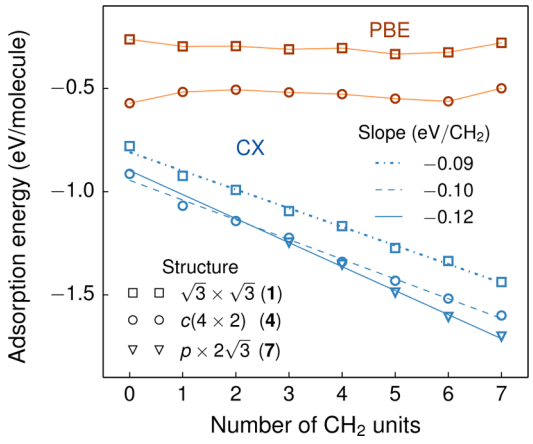

Figure 2. Adsorption energy as a function of the alkyl chain length for both standing-up and lying-down adsorbate geometries. CX reproduces the experimentally observed adsorption energy scaling and predicts a crossing point where adsorption in lying-down geometries becomes energetically favorable. The PBE results show an inconsistent behavior due to the lack of dispersive interactions.

An important observation is the fact that the adsorption energy scaling with chain length is steeper in the LD phase than in the SU phase (Figure 2). For short alkyl chains, a configuration with LD molecules is energetically less favorable than a corresponding SU configuration due to the straining of the Au−S−C bond angle, causing an initial offset in energy in favor of the SU phase. Since the adsorption energy decreases more quickly in the LD phase, there is, however, a crossing point at $n \approx 2$ beyond which adsorption of the thiolates in LD configurations becomes energetically favorable. This is a necessary condition for the thermodynamic stability of the LD phase, but it is not sufficient since structures with different coverages must be compared as a function of (T, p).

Surface Phase Diagram. To study the thermodynamics and interplay between the LD and SU phases for arbitrary (T, p), a convex hull construction based on the surface free energies as calculated from eq 3 was carried out for both MT and HT adsorption on Au(111). The resulting phase stability curves give the minimum value of γ_{ads} as a function of μ_{RS} (Figure 3). To relate these curves to experiment, the temperature range corresponding to that of the chemical potential was evaluated from eq 5 by fixing a pressure $p_{\mathrm{UHV}} = 10^{-13}$ atm typical of the UHV setting in which the LD phases are studied.

For MT in the "$c(4 \times 2)$" structure **4**, CX predicts a phase transition temperature $T_c = 355$ K (Figure 3a) in UHV, above which the clean surface takes over as the stable phase. PBE, on the other hand, yields a lower temperature $T_c = 229$ K for the same transition. A much more striking difference between CX and PBE is observed for HT adsorption; CX yields a region, 489 K < T < 519 K, where the LD structure **8** is the thermodynamically stable phase (Figure 3b), while at the PBE level such a region does not exist. This illustrates, from fully ab initio calculations, how the steeper scaling of the vdW interaction for thiolates adsorbed parallel to the surface ultimately gives rise to the thermodynamic stability of the LD phase. The $(8 \times 2\sqrt{3})$rect structure **7** has an identical stability

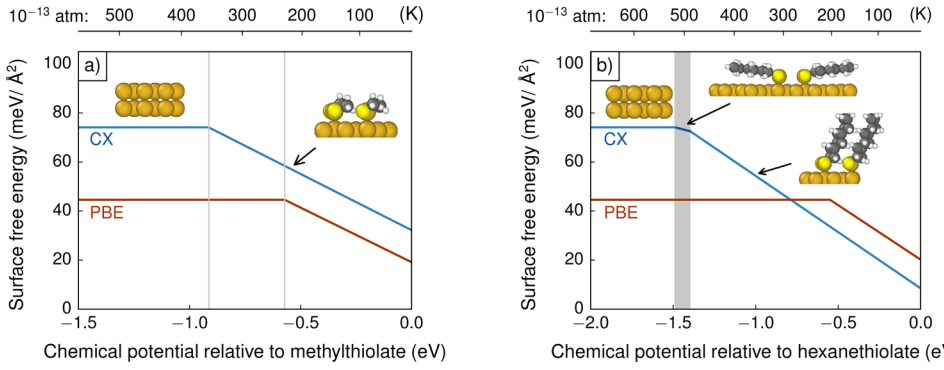

Figure 3. Surface free energy of adsorption γ_{ads} as a function of the chemical potential of the gas phase $\mu^{\mathrm{gas}}_{\mathrm{RS}}$ and temperature for adsorption of (a) methylthiolate and (b) hexanethiolate. In both cases the "$c(4\times 2)$" structure is thermodynamically stable at low temperatures but is eventually taken over by the clean surface as temperature increases. For hexanethiolate an intermediate phase exists where a lying-down (striped) structure is stable. This phase is absent for exchange-correlation functionals which are not dispersion-corrected.

DOI: 10.1021/acs.jpcc.6b03283
J. Phys. Chem. C 2016, 120, 12059−12067

region as **8**, and the difference in energy is below the typical accuracy of DFT calculations. Indeed, STM studies of HT adsorption have revealed the existence of two distinct striped phases, ascribed to structures **5** and **6**,[28,69] which can be thought of as unreconstructed equivalents of **7** and **8**.

The convex hull construction carried out in the case of MT and HT adsorption above can be extended to other chain lengths and used to construct a (n, T) phase diagram in UHV conditions. To avoid the expensive calculations associated with the LD geometries for long thiolates, the linear relations for the adsorption energy scaling (Figure 2) can be used for extrapolation. However, as the chain length increases, one is faced with the complication of having to account for larger contributions from the configurational entropy, S_{conf}. This is expected to be important since molecules in the gas phase have more conformational freedom than on the surface and the number of accessible conformations increases with n. To investigate the impact of S_{conf}, corrections to the chemical potential in eq 5 can be introduced using a rotational isomeric state model. For the molecules in the reservoir, if approximated as thiols rather than dialkyl dithiols, the partition function is given explicitly by eq 6, where the only DFT input needed is the formation energy for a single gauche defect ΔE_g. This energy has a weak dependence on where along the chain the defect occurs, and with CX, the average over the chain is ΔE_g = 31 meV. In contrast, for a thiolate on the surface the formation energy depends critically on where the defect occurs, in particular single defects away from the terminal methyl group are sterically hindered. Close to the end of the chain, the average formation energy for a defect is ΔE_g = 110 meV, which is significantly higher than in the gas phase compared to the average thermal energy at relevant temperatures. As a crude approximation, we therefore neglect the contribution to S_{conf} from the adsorbate molecules entirely and only apply the rotational isomeric state model correction to the chemical potential mentioned above.

The (n, T) phase diagram is shown in Figure 4 where transition temperatures between the SU, LD and clean surface phases have been calculated directly for $n \leq 7$ and then further extrapolated up to n = 15. The phase transition temperatures increase with the chain length, and starting from $n \approx 3$, the LD phase emerges as thermodynamically stable with a stability range that also increases with n. As anticipated, corrections for the configurational entropy lower the phase transition temperatures, but there is still a relatively strong dependence on n and the LD phase stability region is still increasing in size.

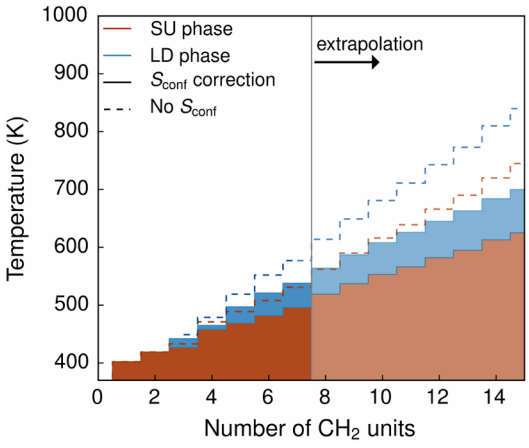

Figure 4. An (n, T) phase diagram for adsorption of alkanethiolates on Au(111). For short chain lengths the only thermodynamically stable phases are the "c(4× 2)" standing-up structure and the clean surface. For medium to long chains there is an additional stable region where the thiolates are in a lying-down (striped) phase.

Comparison to Experiment. For each value of the chain length n, Figure 4 predicts the relative stability, in UHV, as a function of temperature for a set of geometries with coverages corresponding to ordered phases observed in experiments. One way to obtain experimental information on the phase behavior of the system is through TPD measurements, from which it is possible to map out the phase transitions as a function of (T, Θ). For each value of the chain length, the information from Figure 4 could thus be related to regions of stability on a corresponding (T, Θ) diagram, but in practice there are several limitations to consider. First, the phase diagram in Figure 4 is incomplete in the sense that only the LD, SU, and clean surfaces phases are included. In reality, there are very likely additional ordered and disordered phases, e.g., a liquid-like phase lying between the SU phase and the desorbed state. Second, the theoretical calculations rely on the assumption of thermodynamic equilibrium between the adsorbate system and the gas phase. In a desorption experiment, on the other hand, global equilibrium may never be established, and intermediate coverages, typically consisting of coexisting regions of two or more phases,[70] are sampled during the desorption.

Generally, it is possible to combine DFT data with a microkinetic model or a kinetic Monte Carlo algorithm to directly simulate a TPD experiment.[71,72] Such simulations have primarily been carried out for systems with adsorbates without hydrocarbon chains though. For extended thiolates additional complicating factors would arise relating to e.g. the conformational degrees of freedom. Furthermore, a detailed analysis of the dynamics of the melting and desorption of a monolayer could provide further insight into the mechanics underlying many of the experimental observations. The length and time scales involved would, however, require molecular dynamics simulations based on classical force fields. This would not only imply leaving the realm of first-principles calculations but constitute a separate study in its own right.

Keeping the aforementioned limitations in mind, it can still be useful, in the absence of a more detailed analysis using e.g. the simulation methods mentioned above, to compare the phase transition temperatures obtained from Figure 4 to typical experimental desorption temperatures obtained for the SU and LD phases. The trend in our calculations is that T_c increases with n for both transitions $Au_{clean} \rightarrow$ LD and LD $\rightarrow$ SU (Figure 4). The experimental data, on the other hand, are seemingly at odds with this result and indicate that the peak desorption temperatures do not vary appreciably with chain length, with typical values of T_d = 450 K in the SU phase and T_d = 500 K in the LD phase.[62,69,73] A small caveat here is the fact that as demonstrated above, the configurational entropy can significantly alter the phase boundaries for long alkanethiolates in diagrams derived from ab initio calculations. Because of the approximate nature of the correction we applied, there is a higher degree of uncertainty in the phase transition temperatures when the chain extends beyond a few CH_2 units. Furthermore, when comparing the theoretically calculated T_c with the experimentally measured T_d, it must be considered that the latter corresponds to a temperature at which the system has enough thermal energy to overcome the barrier for desorption and will thus depend on the kinetics of the

DOI: 10.1021/acs.jpcc.6b03283
J. Phys. Chem. C 2016, 120, 12059−12067

desorption process. Indeed, experiments have shown that the adsorbates desorb as disulfides from the SU phase while in the LD phase they desorb as thiolate radicals, indicating that the alkyl chains play an important role although the details remain poorly understood. The discrepancy between the TPD desorption temperatures and the theoretical results presented here could be explained by a final desorption barrier that is independent of the chain length. Such a scenario would be possible if, under the given conditions, the dominant desorption channel consists of thiolates at the edge of a patch. We could then envision a multistep desorption process in which a thiolate molecules migrates from the edge with an n-dependent barrier but does not desorb until later, whereby the n-dependence is eliminated.

Some of complications mentioned above can be avoided by focusing on the desorption temperature for methylthiolate where there are no chain length effects. In this case, the CX phase transition temperature T_c = 355 K is significantly closer to the experimental values of around T_d = 450 K compared to the corresponding PBE value of T_c = 229 K. These results indicate that PBE does not give a satisfactory description of the bonding even for methylthiolate where vdW contributions are expected to be small. The remaining discrepancy between CX calculations and the desorption temperature could be indicative of the existence of an energetically more favorable geometry or structure.

CONCLUSIONS

We have investigated the phase diagram of alkanethiolate SAMs on Au(111) by means of dispersion-corrected DFT calculations using the vdW-DF-CX functional and an ab initio thermodynamics model. The main issue addressed is the thermodynamic stability of the lying-down (LD) and standing-up (SU) adsorbate phases for thiolates with medium to long alkyl chains, where the significant contribution from vdW interactions has previously provided a major obstacle for DFT studies.

Based on calculations of the lattice constant and the clean surface energy, CX provides a better description of the bare gold substrate, both compared to PBE as well as the original version of the vdW-DF functional. Nevertheless, in agreement with earlier PBE results, CX favors a reconstructed geometry involving two RS−Au−SR complexes for the "$c(4 \times 2)$" structure. Similarly, in the LD phase, geometries featuring RS−Au−SR complexes arranged in head-to-head configurations are favorable. In the case of hexanethiolate, two structures described by $(8 \times 2\sqrt{3})$rect and $(5\sqrt{3} \times 2\sqrt{3})R30°$ unit cells exhibit similar stability and provide a possible way of reconciling adatom-mediated bonding in the LD phase with STM measurements.

The importance of including dispersive interactions becomes apparent when thiolates with longer alkyl chains are considered. In this case CX shows a stabilizing effect where the adsorption energies decrease linearly with the number of CH_2 units in both the SU and the LD phases. At the PBE level, however, such an effect is completely absent. Furthermore, this linear decrease of the adsorption energy is steeper in the LD phase than in the SU phase; when combined with an ab initio thermodynamics model, this leads to a (T, p)-dependent region of thermodynamic stability for the LD phase. A comparison of the dispersive interaction between the alkyl chain and the substrate to experimental data shows an excellent agreement and indicates the CX is successful in treating all of the interactions in the system on an ab initio basis.

The (n, T) phase diagram, constructed assuming UHV conditions, reveals that the LD phase emerges as stable for thiolates with $n \approx 3$ or more methylene units in the chain. The phase transitions temperatures for both the $Au_{clean} \rightarrow$ LD and LD → SU transitions increase with n and in such a way that the stability region increases in size. We show, however, that this temperature dependence is partly counteracted by the configurational entropy, which is calculated for the gas phase in the rotational isomeric state model using several simplifying assumptions.

In light of the phase diagram, several complications arise in the comparison of ab initio thermodynamics studies to TPD experiments. In particular, the relative insensitivity of TPD desorption temperatures to the chain length could be a consequence of the kinetics of the desorption process, given a two-step mechanism where the final barrier is independent of n.

The present study sheds new light on dispersion-driven phase transitions in thiolated gold systems and also provides a starting point for further experimental and theoretical work aimed at studying self-assembly systems where dispersion effects are important. Some intriguing prospects include for example investigations of solvation effects and the impact of dispersive interactions on protected nanoparticles.[74−76]

AUTHOR INFORMATION

Corresponding Author

*E-mail joalof@chalmers.se; Phone 0046317722902 (J.L.).

Notes

The authors declare no competing financial interest.

ACKNOWLEDGMENTS

This work has been supported by the Knut and Alice Wallenberg foundation, the Swedish Research Council, the Nanoscience and Nanotechnology Area of Advance at Chalmers, and the European Research Council [StG No. 337221-SIMONE, MC-CIG No. 322237]. Computer time allocations by the Swedish National Infrastructure for Computing at NSC (Linköping) and C3SE (Gothenburg) are gratefully acknowledged.

ADDITIONAL NOTE

[a]For the second most stable geometry **3**, there is a corresponding trans configuration that on the basis of STM measurements has been proposed as a candidate for the "$c(4\times 2)$" structure[22] but is 0.04 eV higher in adsorption energy (CX) compared to the cis configuration.

REFERENCES

(1) Ulman, A. Formation and Structure of Self-Assembled Monolayers. *Chem. Rev.* **1996**, *96*, 1533−1554.

(2) Bethell, D.; Brust, M.; Schiffrin, D. J.; Kiely, C. From Monolayers to Nanostructured Materials: An Organic Chemist's View of Self-Assembly. *J. Electroanal. Chem.* **1996**, *409*, 137−143.

(3) Love, J. C.; Wolfe, D. B.; Haasch, R.; Chabinyc, M. L.; Paul, K. E.; Whitesides, G. M.; Nuzzo, R. G. Formation and Structure of Self-Assembled Monolayers of Alkanethiolates on Palladium. *J. Am. Chem. Soc.* **2003**, *125*, 2597−2609.

(4) Schreiber, F. Self-Assembled Monolayers: From 'Simple' Model Systems to Biofunctionalized Interfaces. *J. Phys.: Condens. Matter* **2004**, *16*, R881.

DOI: 10.1021/acs.jpcc.6b03283
J. Phys. Chem. C 2016, 120, 12059−12067

(5) Vericat, C.; Vela, M. E.; Benitez, G.; Carro, P.; Salvarezza, R. C. Self-Assembled Monolayers of Thiols and Dithiols on Gold: New Challenges for a Well-Known System. *Chem. Soc. Rev.* **2010**, *39*, 1805−1834.
(6) Brust, M.; Walker, M.; Bethell, D.; Schiffrin, D. J.; Whyman, R. Synthesis of Thiol-Derivatised Gold Nanoparticles in a Two-Phase Liquid-Liquid System. *J. Chem. Soc., Chem. Commun.* **1994**, *0*, 801−802.
(7) Akola, J.; Walter, M.; Whetten, R. L.; Häkkinen, H.; Grönbeck, H. On the Structure of Thiolate-Protected Au_{25}. *J. Am. Chem. Soc.* **2008**, *130*, 3756−3757.
(8) Jiang, D.-e.; Overbury, S. H.; Dai, S. Structure of $Au_{15}(SR)_{13}$ and Its Implication for the Origin of the Nucleus in Thiolated Gold Nanoclusters. *J. Am. Chem. Soc.* **2013**, *135*, 8786−8789.
(9) Chidsey, C. E. D.; Liu, G.-Y.; Rowntree, P.; Scoles, G. Molecular Order at the Surface of an Organic Monolayer Studied by Low Energy Helium Diffraction. *J. Chem. Phys.* **1989**, *91*, 4421−4423.
(10) Alves, C. A.; Smith, E. L.; Porter, M. D. Atomic Scale Imaging of Alkanethiolate Monolayers at Gold Surfaces with Atomic Force Microscopy. *J. Am. Chem. Soc.* **1992**, *114*, 1222−1227.
(11) Nuzzo, R. G.; Korenic, E. M.; Dubois, L. H. Studies of the Temperature-Dependent Phase Behavior of Long Chain n-Alkyl Thiol Monolayers on Gold. *J. Chem. Phys.* **1990**, *93*, 767−773.
(12) Delamarche, E.; Michel, B.; Kang, H.; Gerber, C. Thermal Stability of Self-Assembled Monolayers. *Langmuir* **1994**, *10*, 4103−4108.
(13) Fenter, P.; Eberhardt, A.; Liang, K. S.; Eisenberger, P. Epitaxy and Chainlength Dependent Strain in Self-Assembled Monolayers. *J. Chem. Phys.* **1997**, *106*, 1600−1608.
(14) Kondoh, H.; Nozoye, H. Low-Temperature Ordered Phase of Methylthiolate Monolayers on Au(111). *J. Phys. Chem. B* **1999**, *103*, 2585−2588.
(15) Voznyy, O.; Dubowski, J. J.; Yates, J. T.; Maksymovych, P. The Role of Gold Adatoms and Stereochemistry in Self-Assembly of Methylthiolate on Au(111). *J. Am. Chem. Soc.* **2009**, *131*, 12989−12993.
(16) Tang, L.; Li, F.; Zhou, W.; Guo, Q. The Structure of Methylthiolate and Ethylthiolate Monolayers on Au(111): Absence of the $(\sqrt{3}\times\sqrt{3})R30°$ Phase. *Surf. Sci.* **2012**, *606*, L31−L35.
(17) Stranick, S. J.; Parikh, A. N.; Allara, D. L.; Weiss, P. S. A New Mechanism for Surface Diffusion: Motion of a Substrate-Adsorbate Complex. *J. Phys. Chem.* **1994**, *98*, 11136−11142.
(18) Molina, L. M.; Hammer, B. Theoretical Study of Thiol-Induced Reconstructions on the Au(111) Surface. *Chem. Phys. Lett.* **2002**, *360*, 264−271.
(19) Morikawa, Y.; Liew, C. C.; Nozoye, H. Methylthiolate Induced Vacancy Formation on Au(111): A Density Functional Theoretical Study. *Surf. Sci.* **2002**, *514*, 389−393.
(20) Roper, M. G.; Skegg, M. P.; Fisher, C. J.; Lee, J. J.; Dhanak, V. R.; Woodruff, D. P.; Jones, R. G. Atop Adsorption Site of Sulphur Head Groups in Gold-Thiolate Self-Assembled Monolayers. *Chem. Phys. Lett.* **2004**, *389*, 87−91.
(21) Yu, M.; Bovet, N.; Satterley, C. J.; Bengió, S.; Lovelock, K. R. J.; Milligan, P. K.; Jones, R. G.; Woodruff, D. P.; Dhanak, V. True Nature of an Archetypal Self-Assembly System: Mobile Au-Thiolate Species on Au(111). *Phys. Rev. Lett.* **2006**, *97*, 166102.
(22) Maksymovych, P.; Sorescu, D. C.; Yates, J. T. Gold-Adatom-Mediated Bonding in Self-Assembled Short-Chain Alkanethiolate Species on the Au(111) Surface. *Phys. Rev. Lett.* **2006**, *97*, 146103.
(23) Grönbeck, H.; Häkkinen, H. Polymerization at the Alkylthiolate-Au(111) Interface. *J. Phys. Chem. B* **2007**, *111*, 3325−3327.
(24) Mazzarello, R.; Cossaro, A.; Verdini, A.; Rousseau, R.; Casalis, L.; Danisman, M. F.; Floreano, L.; Scandolo, S.; Morgante, A.; Scoles, G. Structure of a CH_3S Monolayer on Au(111) Solved by the Interplay Between Molecular Dynamics Calculations and Diffraction Measurements. *Phys. Rev. Lett.* **2007**, *98*, 016102.
(25) Cossaro, A.; Mazzarello, R.; Rousseau, R.; Casalis, L.; Verdini, A.; Kohlmeyer, A.; Floreano, L.; Scandolo, S.; Morgante, A.; Klein, M. L.; et al. X-Ray Diffraction and Computation Yield the Structure of Alkanethiols on Gold(111). *Science* **2008**, *321*, 943−946.
(26) Grönbeck, H.; Häkkinen, H.; Whetten, R. L. Gold-Thiolate Complexes Form a Unique $c(4\times2)$ Structure on Au(111). *J. Phys. Chem. C* **2008**, *112*, 15940−15942.
(27) Grönbeck, H.; Odelius, M. Photoemission Core-Level Shifts Reveal the Thiolate-Au(111) Interface. *Phys. Rev. B: Condens. Matter Mater. Phys.* **2010**, *82*, 085416.
(28) Camillone, N.; Leung, T. Y. B.; Schwartz, P.; Eisenberger, P.; Scoles, G. Chain Length Dependence of the Striped Phases of Alkanethiol Monolayers Self-Assembled on Au(111): An Atomic Beam Diffraction Study. *Langmuir* **1996**, *12*, 2737−2746.
(29) Darling, S. B.; Rosenbaum, A. W.; Wang, Y.; Sibener, S. J. Coexistence of the $(23\times\sqrt{3})$ Au(111) Reconstruction and a Striped Phase Self-Assembled Monolayer. *Langmuir* **2002**, *18*, 7462−7468.
(30) Munuera, C.; Barrena, E.; Ocal, C. Chain-Length Dependence of Metastable Striped Structures of Alkanethiols on Au(111). *Langmuir* **2005**, *21*, 8270−8277.
(31) Shimada, T.; Kondoh, H.; Nakai, I.; Nagasaka, M.; Yokota, R.; Amemiya, K.; Ohta, T. Structural Study of Hexanethiolate on Au(111) in the 'Striped' Phase. *Chem. Phys. Lett.* **2005**, *406*, 232−236.
(32) Balzer, F.; Gerlach, R.; Polanski, G.; Rubahn, H. G. Chain Length Dependence of the Structure of Alkane Thiol Films on Au(111). *Chem. Phys. Lett.* **1997**, *274*, 145−151.
(33) Furche, F. Molecular Tests of the Random Phase Approximation to the Exchange-Correlation Energy Functional. *Phys. Rev. B: Condens. Matter Mater. Phys.* **2001**, *64*, 195120.
(34) Becke, A. D.; Johnson, E. R. A Density-Functional Model of the Dispersion Interaction. *J. Chem. Phys.* **2005**, *123*, 154101.
(35) Grimme, S. Semiempirical GGA-Type Density Functional Constructed with a Long-Range Dispersion Correction. *J. Comput. Chem.* **2006**, *27*, 1787−1799.
(36) Tkatchenko, A.; Scheffler, M. Accurate Molecular Van Der Waals Interactions from Ground-State Electron Density and Free-Atom Reference Data. *Phys. Rev. Lett.* **2009**, *102*, 073005.
(37) Tkatchenko, A.; DiStasio, R. A.; Car, R.; Scheffler, M. Accurate and Efficient Method for Many-Body van der Waals Interactions. *Phys. Rev. Lett.* **2012**, *108*, 236402.
(38) Dion, M.; Rydberg, H.; Schröder, E.; Langreth, D. C.; Lundqvist, B. I. Van der Waals Density Functional for General Geometries. *Phys. Rev. Lett.* **2004**, *92*, 246401.
(39) Klimeš, J.; Bowler, D. R.; Michaelides, A. Chemical Accuracy for the van der Waals Density Functional. *J. Phys.: Condens. Matter* **2010**, *22*, 022201.
(40) Klimeš, J.; Bowler, D. R.; Michaelides, A. Van der Waals Density Functionals Applied to Solids. *Phys. Rev. B: Condens. Matter Mater. Phys.* **2011**, *83*, 195131.
(41) Berland, K.; Cooper, V. R.; Lee, K.; Schröder, E.; Thonhauser, T.; Hyldgaard, P.; Lundqvist, B. I. Van der Waals Forces in Density Functional Theory: A Review of the vdW-DF Method. *Rep. Prog. Phys.* **2015**, *78*, 066501.
(42) Carro, P.; Salvarezza, R.; Torres, D.; Illas, F. On the Thermodynamic Stability of $(\sqrt{3}\times\sqrt{3})R30°$ Methanethiolate Lattice on Reconstructed Au(111) Surface Models. *J. Phys. Chem. C* **2008**, *112*, 19121−19124.
(43) Abufager, P. N.; Canchaya, J. G. S.; Wang, Y.; Alcamí, M.; Martín, F.; Soria, L. A.; Martiarena, M. L.; Reuter, K.; Busnengo, H. F. Theoretical Study of the Structure of Self-Assembled Monolayers of Short Alkylthiolates on Au(111) and Ag(111): The Role of Induced Substrate Reconstruction and chain-chain Interactions. *Phys. Chem. Chem. Phys.* **2011**, *13*, 9353−9362.
(44) Wang, X.-G.; Weiss, W.; Shaikhutdinov, S. K.; Ritter, M.; Petersen, M.; Wagner, F.; Schlögl, R.; Scheffler, M. The Hematite (α−Fe_2O_3)(0001) Surface: Evidence for Domains of Distinct Chemistry. *Phys. Rev. Lett.* **1998**, *81*, 1038−1041.
(45) Wang, X.-G.; Chaka, A.; Scheffler, M. Effect of the Environment on α−Al_2O_3(0001) Surface Structures. *Phys. Rev. Lett.* **2000**, *84*, 3650−3653.

DOI: 10.1021/acs.jpcc.6b03283
J. Phys. Chem. C 2016, 120, 12059−12067

(46) Reuter, K.; Scheffler, M. Composition, Structure, and Stability of RuO_2(110) As a Function of Oxygen Pressure. *Phys. Rev. B: Condens. Matter Mater. Phys.* **2001**, *65*, 035406.
(47) Ferrighi, L.; Pan, Y.-x.; Grönbeck, H.; Hammer, B. Study of Alkylthiolate Self-Assembled Monolayers on Au(111) Using a Semilocal Meta-GGA Density Functional. *J. Phys. Chem. C* **2012**, *116*, 7374−7379.
(48) Berland, K.; Hyldgaard, P. Exchange Functional That Tests the Robustness of the Plasmon Description of the van der Waals Density Functional. *Phys. Rev. B: Condens. Matter Mater. Phys.* **2014**, *89*, 035412.
(49) Torres, E.; Blumenau, A. T.; Biedermann, P. U. Steric and Chain Length Effects in the $(\sqrt{3}\times\sqrt{3})R30°$ Structures of Alkanethiol Self-Assembled Monolayers on Au(111). *ChemPhysChem* **2011**, *12*, 999−1009.
(50) Carro, P.; Torrelles, X.; Salvarezza, R. C. A Novel Model for the $(\sqrt{3} \times \sqrt{3})R30°$ Alkanethiolate-Au(111) Phase Based on Alkanethiolate-Au Adatom Complexes. *Phys. Chem. Chem. Phys.* **2014**, *16*, 19017−19023.
(51) Würflinger, A. A Simple Recursion Formula for the Calculation of Conformational Properties of n-Alkanes. *Mol. Phys.* **1983**, *49*, 413−420.
(52) Würflinger, A. Conformational Properties of n-Alkanes. *Colloid Polym. Sci.* **1984**, *262*, 115−118.
(53) Kresse, G.; Hafner, J. Ab Initio Molecular Dynamics for Liquid Metals. *Phys. Rev. B: Condens. Matter Mater. Phys.* **1993**, *47*, 558−561.
(54) Kresse, G.; Furthmüller, J. Efficient Iterative Schemes for Ab Initio Total-Energy Calculations Using a Plane-Wave Basis Set. *Phys. Rev. B: Condens. Matter Mater. Phys.* **1996**, *54*, 11169−11186.
(55) Blöchl, P. E. Projector Augmented-Wave Method. *Phys. Rev. B: Condens. Matter Mater. Phys.* **1994**, *50*, 17953−17979.
(56) Kresse, G.; Joubert, D. From Ultrasoft Pseudopotentials to the Projector Augmented-Wave Method. *Phys. Rev. B: Condens. Matter Mater. Phys.* **1999**, *59*, 1758−1775.
(57) Björkman, T. Testing Several Recent van der Waals Density Functionals for Layered Structures. *J. Chem. Phys.* **2014**, *141*, 074708.
(58) Perdew, J. P.; Burke, K.; Ernzerhof, M. Generalized Gradient Approximation Made Simple. *Phys. Rev. Lett.* **1996**, *77*, 3865−3868.
(59) Stukowski, A. Visualization and Analysis of Atomistic Simulation Data with OVITO-the Open Visualization Tool. *Modell. Simul. Mater. Sci. Eng.* **2010**, *18*, 015012.
(60) Pearson, W. B. In *A Handbook of Lattice Spacings and Structures of Metals and Alloys*; Pearson, W. B., Ed.; International Series of Monographs on Metal Physics and Physical Metallurgy; Pergamon: 1958; Vol. *4*, pp 123−130.
(61) Tyson, W. R.; Miller, W. A. Surface Free Energies of Solid Metals: Estimation from Liquid Surface Tension Measurements. *Surf. Sci.* **1977**, *62*, 267−276.
(62) Nuzzo, R. G.; Zegarski, B. R.; Dubois, L. H. Fundamental Studies of the Chemisorption of Organosulfur Compounds on Gold(111). Implications for Molecular Self-Assembly on Gold Surfaces. *J. Am. Chem. Soc.* **1987**, *109*, 733−740.
(63) Wang, J.-g.; Selloni, A. The $c(4\times 2)$ Structure of Short- and Intermediate-Chain Length Alkanethiolate Monolayers on Au(111): A DFT Study. *J. Phys. Chem. C* **2007**, *111*, 12149−12151.
(64) Carro, P.; Pensa, E.; Vericat, C.; Salvarezza, R. C. Hydrocarbon Chain Length Induces Surface Structure Transitions in Alkanethiolate-Gold Adatom Self-Assembled Monolayers on Au(111). *J. Phys. Chem. C* **2013**, *117*, 2160−2165.
(65) Lavrich, D. J.; Wetterer, S. M.; Bernasek, S. L.; Scoles, G. Physisorption and Chemisorption of Alkanethiols and Alkyl Sulfides on Au(111). *J. Phys. Chem. B* **1998**, *102*, 3456−3465.
(66) Wang, Y.; Chi, Q.; Hush, N. S.; Reimers, J. R.; Zhang, J.; Ulstrup, J. Gold Mining by Alkanethiol Radicals: Vacancies and Pits in the Self-Assembled Monolayers of 1-Propanethiol and 1-Butanethiol on Au(111). *J. Phys. Chem. C* **2011**, *115*, 10630−10639.
(67) Li, F.; Tang, L.; Voznyy, O.; Gao, J.; Guo, Q. The Striped Phases of Ethylthiolate Monolayers on the Au(111) Surface: A Scanning Tunneling Microscopy Study. *J. Chem. Phys.* **2013**, *138*, 194707.
(68) Woodruff, D. P. The Interface Structure of n-Alkylthiolate Self-Assembled Monolayers on Coinage Metal Surfaces. *Phys. Chem. Chem. Phys.* **2008**, *10*, 7211−7221.
(69) Kondoh, H.; Kodama, C.; Sumida, H.; Nozoye, H. Molecular Processes of Adsorption and Desorption of Alkanethiol Monolayers on Au(111). *J. Chem. Phys.* **1999**, *111*, 1175−1184.
(70) Schreiber, F.; Eberhardt, A.; Leung, T. Y. B.; Schwartz, P.; Wetterer, S. M.; Lavrich, D. J.; Berman, L.; Fenter, P.; Eisenberger, P.; Scoles, G. Adsorption Mechanisms, Structures, and Growth Regimes of an Archetypal Self-Assembling System: Decanethiol on Au(111). *Phys. Rev. B: Condens. Matter Mater. Phys.* **1998**, *57*, 12476−12481.
(71) Zuniga-Hansen, N.; Calbi, M. M. Thermal Desorption from Heterogeneous Surfaces. *J. Phys. Chem. C* **2012**, *116*, 5025−5032.
(72) Wang, C.-C.; Wu, J.-Y.; Jiang, J.-C. Microkinetic Simulation of Temperature-Programmed Desorption. *J. Phys. Chem. C* **2013**, *117*, 6136−6142.
(73) Stettner, J.; Winkler, A. Characterization of Alkanethiol Self-Assembled Monolayers on Gold by Thermal Desorption Spectroscopy. *Langmuir* **2010**, *26*, 9659−9665.
(74) Kumara, C.; Zuo, X.; Ilavsky, J.; Chapman, K. W.; Cullen, D. A.; Dass, A. Super-Stable, Highly Monodisperse Plasmonic Faradaurate-500 Nanocrystals with 500 Gold Atoms: au$_{\sim}$500(SR)$_{\sim}$120. *J. Am. Chem. Soc.* **2014**, *136*, 7410−7417.
(75) Ouyang, R.; Jiang, D.-e. Ligand-Conformation Energy Landscape of Thiolate-Protected Gold Nanoclusters. *J. Phys. Chem. C* **2015**, *119*, 21555−21560.
(76) Reimers, J. R.; Ford, M. J.; Halder, A.; Ulstrup, J.; Hush, N. S. Gold Surfaces and Nanoparticles Are Protected by Au(0)-Thiyl Species and Are Destroyed When Au(I)-Thiolates Form. *Proc. Natl. Acad. Sci. U. S. A.* **2016**, *113*, E1424.

DOI: 10.1021/acs.jpcc.6b03283
J. Phys. Chem. C 2016, 120, 12059−12067